Protein Conformation Change of Myoglobin upon Ligand Binding Probed by Ultraviolet Resonance Raman Spectroscopy†

Nami Haruta,‡ Michihiko Aki,‡ Shin-ichi Ozaki,§,|| Yoshihito Watanabe,‡,§ and Teizo Kitagawa*,‡,⊥

School of Mathematical and Physical Sciences, The Graduate University for Advanced Studies, and Institute for Molecular Science and Center for Integrative Bioscience, Okazaki National Research Institutes, Myodaiji, Okazaki, 444-8585 Japan

Received November 16, 2000; Revised Manuscript Received March 28, 2001

ABSTRACT: Conformational change of myoglobin (Mb) accompanied by binding of a ligand was investigated with 244 nm excited ultraviolet resonance Raman Spectroscopy (UVRR). The UVRR spectra of native sperm whale (sw) and horse (h) Mbs and W7F and W14F swMb mutants for the deoxy and CO-bound states enabled us to reveal the UVRR spectra of Trp7, Trp14, and Tyr151 residues, separately. The difference spectra between the deoxy and CO-bound states reflected the environmental or structural changes of Trp and Tyr residues upon CO binding. The W3 band of Trp7 near the N-terminus exhibited a change upon CO binding, while Trp14 did not. Tyr151 in the C-terminus also exhibited a definite change upon CO binding, but Tyr103 and Tyr146 did not. The spectral change of Tyr residues was characterized through solvent effects of a model compound. The corresponding spectral differences between CO- and *n*-butyl isocyanide-bound forms were much smaller than those between the deoxy and CO-bound forms, suggesting that the conformation change in the C- and N-terminal regions is induced by the proximal side of the heme through the movement of iron. Although the swinging up of His64 upon binding of a bulky ligand is noted by X-ray crystallographic analysis, UVRR spectra of His for the *n*-butyl isocyanide-bound form did not detect the exposure of His64 to solvent.

Signal transduction in a biological system becomes increasingly important, and elucidation of its structural mechanism is a current topic in basic biochemistry (*1*). Many sensor proteins for diatomic molecules including CooA (transcriptional factor) for CO (*2*), FixL (histidine kinase) for O_2 (*3*), soluble guanylate cyclase (GTP → cGMP) for NO (*4*), and Dos protein for O_2 (*5*) are heme proteins which recognize a specific diatomic molecule by its binding to the heme iron, and subsequent conformational changes of a protein result in a functional reaction at the catalytic site. Therefore, thorough elucidation of a structural change of protein upon ligand binding to heme is essential to interpret mechanisms of these proteins. We have selected myoglobin (Mb)[1] as a model molecule for exploring this problem, because Mb binds O_2, CO, and NO, and there are many physicochemical studies along this line including the applications of X-ray crystallographic analysis (*6*) and of NMR (*7*), IR (*8*), and resonance Raman (*9*) techniques to various mutant proteins as well as the native one.

Kinetic studies and X-ray crystallographic analysis combined with mutagenesis pointed out that the distal side residues including H64, V68, L29, and F43 control the affinity of the exogenous diatomic ligand (*10*, *11*). The general concepts for recognition of an exogenous molecule in ligand binding have been worked out (*12*), but there are only a few studies about overall conformation changes induced by ligand binding (*13*−*15*). A pathway of an exogenous ligand from solvent to the buried binding site is formed when distal His is swung up outward. This structure is referred as the open conformation which can be seen stationary upon protonation of distal His (*16*, *17*), binding of a bulky ligand (*18*−*20*), and mutation of F46 (*21*) and transiently upon photodissociation of CO (*22*).

Mb is a typical α-helical protein (∼80%) with eight helices labeled A through H. A single heme is embedded between the E and F helices and connected directly to the protein through a covalent bond between His93 (proximal His) and the heme iron. The heme iron moves out of the heme plane toward His93 by 0.3 Å (*6*) in the deoxy state, while it stays in the porphyrin plane in the ligand-bound form. This movement of the iron atom is considered to serve as a trigger of the T−R transition of hemoglobin (Hb), because it accompanies movement of proximal His (F8) and accordingly induces the movement of the F helix containing F8 His. Then, the A helix, which is hydrogen bonded with the E helix and contains the N-terminus, is dislocated (*23*).

† This work was supported in part by Grant-in-Aid for Scientific Research in Priority Area to T.K. (12045264) from the Ministry of Education, Science, Culture, and Sports of Japan.

* To whom correspondence should be addressed. Phone: +81-564-55-7340. Fax: +81-564-55-4639. E-mail: teizo@ims.ac.jp.

‡ The Graduate University for Advanced Studies.

§ Institute for Molecular Science, Okazaki National Research Institutes.

|| Present address: Faculty of Education, Yamagata University, Yamagata, 990-8560 Japan.

⊥ Center for Integrative Bioscience, Okazaki National Research Institutes.

[1] Abbreviations: Mb, myoglobin; Hb, hemoglobin; RR, resonance Raman; UVRR, ultraviolet resonance Raman; Fe(PP), iron protoporphyrin IX; CTAB, cetyltrimethylammonium bromide; 2-MeIm, 2-methylimidazole; HMPA, hexamethylphosphoric triamide; MES, 2-(*N*-morpholino)ethanesulfonic acid; Fe(II)(PP)(2-MeIm), 2-MeIm adduct of Fe(II)(PP); COFe(II)(PP)(2-MeIm), CO adduct of Fe(II)(PP)(2-MeIm).

10.1021/bi002640k CCC: $20.00
Published on Web 05/18/2001

Conversely, the strain of the protein produced by the intersubunit interactions is reflected by the strength of the Fe−N (F8) bond, which has good correlation with the O_2 affinity (*24*). Consequently, the Fe−His stretching frequency can serve as a marker of quaternary structure of Hb (*25*).

The picosecond IR study by Causprove and Dyer (*13*) demonstrated that a change of protein backbone structure probed by amide I is almost completed in 50 ps after photolysis of CO. The geminate recombination rate of CO to the photodissociated unrelaxed species is distinctly faster than the rate to the equilibrium deoxyMb (*14*), indicating that the small conformational change is functionally significant. Although a fluorescence decay time of Trp7 is reported to be different between deoxyMb and COMb (*15*), little is known about their structural differences.

Resonance Raman (RR) spectroscopy is a powerful tool to monitor a structure of the chromophore molecule in the protein (*25*). Particularly, UV resonance Raman (UVRR) spectra are useful to monitor protein structural changes (*26*). Upon excitation around 220−250 nm, side chain vibrations of tyrosine and tryptophan residues are selectively intensity enhanced, while amide modes reflecting the secondary structure are dominant upon excitation around 200 nm (*27*). UVRR bands of Trp and Tyr residues reflect not only their hydrophobic/hydrophilic surroundings but also hydrogen bonding (*28*). Some modes of protonated histidine can also be enhanced by 244 nm excitation only for D_2O solutions (*29*, *30*). Accordingly, in this study, we applied UVRR spectroscopy to Mb and its mutants to explore structural change upon ligand binding through spectral changes of Tyr and Trp bands and tried to detect the open form with the signal of protonated His64 in D_2O solution.

MATERIALS AND METHODS

Procedures for Protein Sample Preparation. Native sperm whale Mb (swMb, Biozyme) and horse Mb (hMb, Sigma) were dissolved in 25 mM potassium phosphate (K-P) buffer, pH 6.0, containing potassium ferricyanide. After gel filtration through Sephadex 25G (Amersham Pharmacia Biotech), the Mb solution was loaded on a CM52 column (Whatman), which had been equilibrated with 25 mM phosphate buffer, pH 6.0, and eluted by a linear gradient with 50 mM K-P buffer, pH 9.0. The buffer was changed finally to 50 mM K-P buffer, pH 7.0. DeoxyMb and COMb were prepared by addition of sodium dithionite (final concentration 2 mM) after replacement of the air inside the cell with N_2 and CO, respectively. To obtain the *n*-butyl isocyanide (*n*-BuIC) adduct of Mb (*n*-BuICMb), *n*-BuIC (Aldrich Chemical Co.) was added to the 370 μM Mb solution in the 50 mM K-P buffer (pH 7.0) to make the final concentration of *n*-BuIC 2.4 mM. To get a D_2O solution of Mb, lyophilized hMb (Sigma) was dissolved in the 50 mM D_2O solution of MES (Dojin Chemicals).

The expression and purification of W7F and W14F mutants were performed according to the method described by Springer (*31*), with some modifications. The mutation of a sequence coding Mb between *Kpn*I and *Pst*I restriction sites of the pUC19 vector was introduced by the PCR-based technique. The cell pellet incubated overnight at 37 °C was disrupted by sonication, and a red crude extract was applied to ammonium sulfate fractionation, anion-exchange chromatography with DE52 (Whatman), and finally cation-exchange chromatography (CM52) as described above.

Preparation of Iron Porphyrin Complexes and Others. The ferrous five- or six-coordinate iron protoporphyrin IX [Fe(II)(PP)] was prepared by dissolving hemin (Sigma) in 0.1 M NaOH solution followed by dilution to the final porphyrin concentration of 0.5 mM with 50 mM K-P buffer, pH 7.0, containing 1% cetyltrimethylammonium bromide (CTAB) and 20 mM 2-methylimidazole (2-MeIm). Reduction of this solution with sodium dithionite under a N_2 and CO atmosphere yielded the five-coordinated high-spin Fe(II)(PP)(2-MeIm) and six-coordinated low-spin COFe(II)(PP)(2-MeIm), respectively. The formations of these complexes were confirmed by the Q-band of their absorption spectra.

N-Acetyltyrosine ethyl ester (Aldrich) and hexamethylphosphoric triamide (HMPA, Aldrich) were used as purchased. *N*-Acetyltyrosine ethyl ester was dissolved into propanol to yield a 100 mM solution which was used as a stock solution. For every use the stock solution was diluted with cyclohexane or distilled water at various ratios. Raman bands of propanol and cyclohexane were used to normalize the spectral intensity. HMPA was added to yield a 2% (v/v) solution.

UVRR Measurements. The UVRR excitation source at 244 nm was generated by frequency doubling of the 488 nm fundamental line of an Ar^+ ion laser, which was mode-locked at 80 MHz. About 150 μL aliquot of the sample solution was placed into a spinning cell with a stirring function (*32*). Raman scattered light at right angles was collected with a UV microscope objective lens, dispersed with a 126 cm single monochromator (Spex1269) equipped with a 3600 groove/mm holographic grating, and detected by an intensified charge-coupled detector (ICCD, Princeton Instruments, model ICCD-1024MG-E/1). Details of the measurement system are explained elsewhere (*32*). The spectral resolution was 6.9 cm^{-1} for 244 nm excitation. The laser power at the sample point was 0.12−0.2 mW, and the total exposure time to get one spectrum was about 1 h or slightly longer.

The integrity of sample after exposure to UV laser light was confirmed by comparing the visible absorption spectra measured before and after the UVRR measurements. To standardize the Raman intensity, the Mb solution containing 100 mM Na_2SO_4 was measured repeatedly. It was found through such measurements that the intensity of the sulfate band at 982 cm^{-1} always reproduced its peak height among the samples from the same solution when the curve slopes at both sides of the spectral region (back ground) were adjusted. To avoid possible salt effects on Mb structures, the intensity standardization for various Mb solutions was carried out using the curve slope adjustment at both sides for the spectra obtained under a certain fixed instrumental condition.

RESULTS

Figure 1 shows the 244 nm excited UVRR spectra of sperm whale Mb in the deoxy (A), CO-bound (B), and *n*-BuIC-bound forms (C). Spectra D and E delineate the difference spectra, that is, deoxyMb − COMb and deoxyMb − *n*-BuICMb. Since *n*-BuIC has a bulky alkyl chain and X-ray crystallographic results indicated the swung up geometry of His64 for it (*20*), some differences are expected

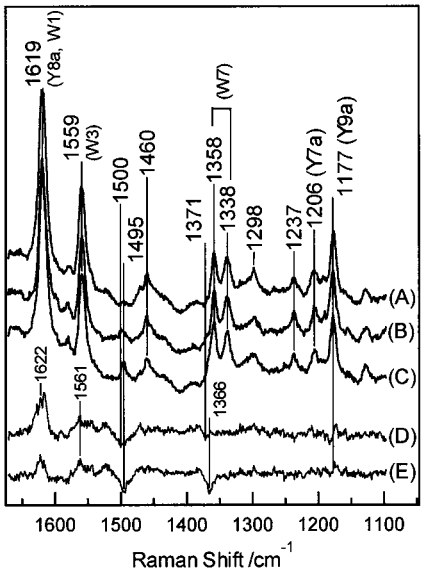

FIGURE 1: The 244 nm excited UVRR spectra of deoxy Mb (A), COMb (B), and *n*-BuICMb (C) of native swMb. Spectra D and E are differences, (A) minus (B) and (A) minus (C), respectively. The protein concentration was 370 μM in 50 mM potassium phosphate buffer, pH 7.0. *n*-BuICMb was derived by adding *n*-butyl isocyanide to the deoxyMb solution to yield its final concentration of 2.4 mM at pH 7.0. The laser power at the sample point was 0.12 mW, and the total exposure time was 60 min.

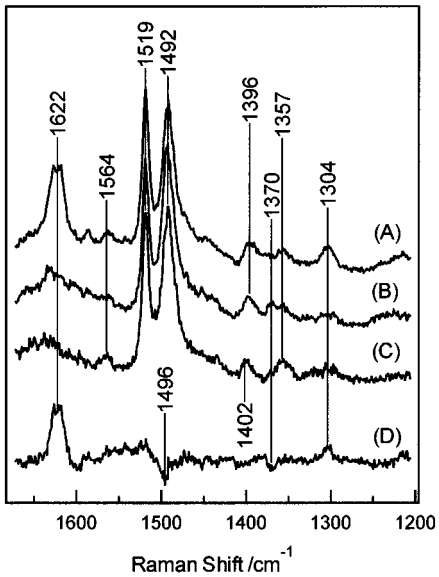

FIGURE 2: UVRR spectra of iron(II) protoporphyrin IX−2-methylimidazole complexes in 50 mM borate buffer, pH 8.0, containing 1% CTAB and 20 mM 2-MeIm: five-coordinate deoxy form (A), six-coordinate CO-bound form (B), and their difference [D = (A) − (B)]. Spectrum C denotes the spectrum of solvent containing 1% CTAB and 20 mM 2-MeIm. The concentration of iron porphyrin was 500 μM.

if steric interaction at the distal pocket is the origin of structural changes. The 244 nm excited Raman spectra are dominated by contributions from Trp and Tyr residues. The Raman bands arising from Trp and Tyr residues are assigned according to Harada and co-workers (*28*) and labeled W and Y, respectively. Trp bands are observed at 1619 (W1 overlapped with Y8a), 1559 (W3), 1460 (W5), 1358−1338 (W7, tryptophan doublet), and 1237 cm^{-1} (W10). The UVRR bands of Tyr are observed at 1619 (Y8a), 1206 (Y7a), and 1177 cm^{-1} (Y9a).

The difference spectrum between deoxy and CO-bound states (Figure 1D) indicates that the intensities of the W1 and/or Y8a and W3 bands of Trp become weaker upon binding of a ligand, and the frequency of Y9a of Tyr is shifted. The spectral changes are qualitatively the same between traces D and E, suggesting that the structural change is not caused by steric repulsion between the bound ligand and nearby residues. In both difference spectra, there are some peaks that cannot be assigned to Trp and Tyr bands. To clarify the origin of such bands, UVRR spectra of Fe(II)(PP)(2-MeIm) and COFe(II)(PP)(2-MeIm) were examined.

Figure 2 shows UVRR spectra of five-coordinated high-spin Fe(II)(PP)(2-MeIm) (A), six-coordinated low-spin COFe(II)(PP)(2-MeIm) (B), and the solvent (C) containing 2-MeIm and 1% CTAB. Fe(II)(PP)(2-MeIm) and COFe(II)(PP)(2-MeIm) can be regarded as model compounds of the heme moiety of deoxyMb and COMb, respectively. 2-Methylimidazole is presumably under preresonance upon excitation at 244 nm and, accordingly, gave many Raman bands (at 1564, 1519, 1492, 1402, and 1357 cm^{-1}) at pH 8.3. The relative intensities of two strong bands at 1492 and 1519 cm^{-1} were sensitive to pH, because the former and the latter were derived from an imidazole and an imidazolium ion, respectively.

The difference spectrum (Figure 2D), five-coordinate minus six-coordinate complexes, exhibits positive peaks at 1622 and 1304 cm^{-1} and negative ones at 1496 and 1370 cm^{-1}. Since the contributions from free 2-MeIm and CTAB should be completely canceled in the difference spectrum, these difference peaks must arise from the heme. Accordingly, the negative peaks at 1496 and 1370 cm^{-1} and the positive peaks at 1622 and 1304 cm^{-1} in trace D are assigned to the bands of the CO-bound and deoxy forms of iron porphyrin, respectively. It is clear that the difference peak at 1560 cm^{-1} in Figure 1 arises from changes of Trp residues, but it is necessary to subtract the difference spectrum of the heme (Figure 2D) from the observed deoxyMb minus COMb UVRR spectra to abstract the contribution of the globin moiety for bands overlapped with the porphyrin bands. Note that Tyr bands are not overlapped with porphyrin bands.

Although swMb has three Tyr residues (Tyr103, Tyr146, and Tyr151), most of mammalian Mbs have two Tyr residues, that is, Tyr103 and Tyr146. To determine the Raman contribution of Tyr151, the UVRR spectra of hMb were examined. Traces A and B of Figure 3 show the 244 nm excited RR spectra of deoxyMb and COMb, respectively, and traces C, D, and E delineate the difference spectra, deoxy minus CO forms, of swMb, hMb, and the model compound, respectively. Apparently, the deoxy minus CO difference spectra of hMb and swMb are alike regarding bands at 1620, 1560, 1497, and 1370 cm^{-1} bands, to which the heme moiety also seems to contribute. The inset of Figure 3 shows the expanded spectra of swMb and hMb in the frequency region of 1230−1140 cm^{-1}, where the Y7a (1208 cm^{-1}) and Y9a (1177 cm^{-1}) bands appear.

The solid and broken lines in the upper two spectra of the inset show the raw spectra of the deoxy and CO-bound forms, respectively, and the lower two curves represent the deoxy minus CO difference spectra of swMb (SW) and hMb (Horse). It is clear that the differential peak at 1177 cm^{-1}

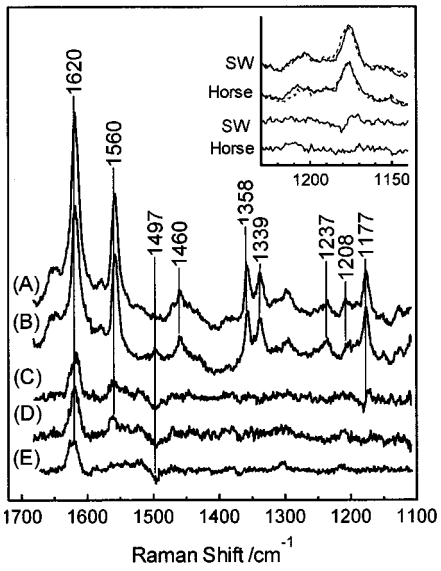

FIGURE 3: UVRR spectra of the deoxy (A) and CO-bound (B) forms of hMb excited at 244 nm. Spectra C, D, and E represent the differences, deoxy minus CO spectra of swMb, hMb, and the 2-MeIm adduct of iron porphyrin, respectively. The inset shows the expanded spectra in the Y7a and Y9a region of swMb and hMb. The top and second traces delineate the raw spectra of swMb and hMb, respectively, in which solid lines and broken lines denote the deoxy and CO-bound forms, respectively. The third and fourth traces indicate the deoxy minus CO difference spectra of swMb and hMb, respectively.

(Y9a) is present for swMb but absent for hMb, indicating that the Tyr difference band of swMb arises from Tyr151. Except for this differential peak, spectra C and D are quite similar. This means that Tyr146 undergoes no environmental change upon ligand binding despite of its proximity to Tyr151. Although the X-ray structural analyses of swMb and hMb pointed out the presence of four different regions between the two proteins (*33*), those regions seem to have no influence on the vibrational spectra of Tyr and Trp residues. To get insight into the structural change of Tyr151, seen for swMb upon CO binding in Figure 3C, the solvent dependence of the UVRR spectrum of a model compound of Tyr residue was investigated.

Figure 4a shows the UVRR spectra in the 1150−1250 cm^{-1} region of *N*-acetyltyrosine ethyl ester, which is a model compound of the Tyr residue. This compound is soluble in water−organic mixed as well as neat organic solvents, and accordingly solvent effects of RR spectra could be examined. In Figure 4a, hydrophobicity of solvent decreases from A toward E. Although three Tyr bands including Y9a (1177 cm^{-1}), Y7a (1205 cm^{-1}), and Y7a′ (∼1250 cm^{-1}) are expected to appear in this region, the intensity of Y7a′ is very weak upon excitation at 244 nm. The absolute intensities of the Y7a and Y9a bands excited at 244 nm decrease, and their peaks shift to higher frequencies as hydrophobicity decreases. Moreover, their relative intensities, Y9a/Y7a, exhibit a good correlation with the hydrophilic/hydrophobic environment as plotted in Figure 4b. It is noted, however, that *N*-acetyltyrosine ethyl ester was not soluble in pure cyclohexane to the extent to yield a Raman band, but it became soluble in cyclohexane mixed with a small amount of propanol, giving rise to the intense Y9a band (spectrum A). When a strong proton acceptor, HMPA, was added to this mixed solvent, the Y9a band became much stronger, as

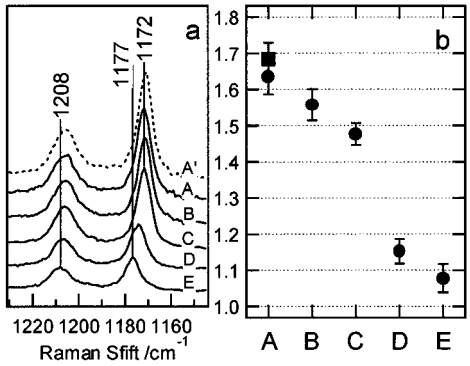

FIGURE 4: Solvent effects on the Y9a and Y7a bands of *N*-acetyltyrosine ethyl ester (panel a) and the Y9a/Y7a intensity ratio (panel b). Solvents: (A) cyclohexane:propanol = 9:1, (B) cyclohexane:propanol = 1:1, (C) neat propanol, (D) propanol:water = 1:1, and (E) propanol:water = 1:9. Spectrum A′ in panel a and the square in panel b denote the case in which a strong proton acceptor (HMPA) was added to mixture A with a concentration of 2.0% (v/v).

depicted by spectrum A′. Thus, it would be more precise to suggest that the Y9a band becomes stronger when phenolic hydrogen serves as a hydrogen bond donor in hydrophobic environments.

Intensities of the Y9a band of hMb in the deoxy and CO-bound states, shown in traces A and B of Figure 3, respectively, are fairly strong. According to the solvent effect of the Tyr model compound, Tyr103 and Tyr146 are deduced to stay in hydrophobic environments and to serve as a hydrogen bond donor. Since the intensities of Y7a and Y9a were nearly the same in the swMb minus hMb difference spectrum (data not shown), the environment of Tyr151 is inferred to be hydrophilic on the basis of Figure 4b. The studies of pH titration with absorption spectra (*34*) and X-ray crystal structures (*6*) indicate that Tyr151 is exposed to solvent. Consequently, the UVRR results for a solution are consonant with the X-ray results for crystals.

As noted for Figure 3, the intensity of the 1560 cm^{-1} band of Trp changes upon CO binding. swMb has two Trp residues, Trp7 and Trp14, which are both on the A helix and are highly conserved. To determine which Trp residue undergoes environmental changes upon ligand binding, we tried to isolate a spectrum of individual Trp residues by preparing two mutants, W7F and W14F. These two mutants had correct folding, since their absorption spectra were the same as that of native Mb, and the 244 nm excited UVRR spectra were quite similar to that of native Mb except for the bands derived from Trp residues. Figure 5a displays the raw UVRR spectra of the deoxy (solid lines) and CO-bound forms (broken lines) of native swMb (A) and the W14F (B), and W7F (C) swMb mutants. The ordinate scales of all spectra are normalized with Tyr bands, Y7a and Y9a, which are different between deoxyMb and MbCO but are the same among the three spectra.

Accordingly, in their deoxy minus CO difference spectra delineated in Figure 5b, the magnitudes of differential patterns at Y9a of traces A, B, and C are alike. Nevertheless, the magnitudes of difference peaks of Trp at 1561 cm^{-1} are different among them. Note that spectra B and C in Figure 5b represent the environmental changes of Trp7 and Trp14, respectively, while spectrum A reflects the sum of both. Spectrum D depicts the deoxy minus CO difference

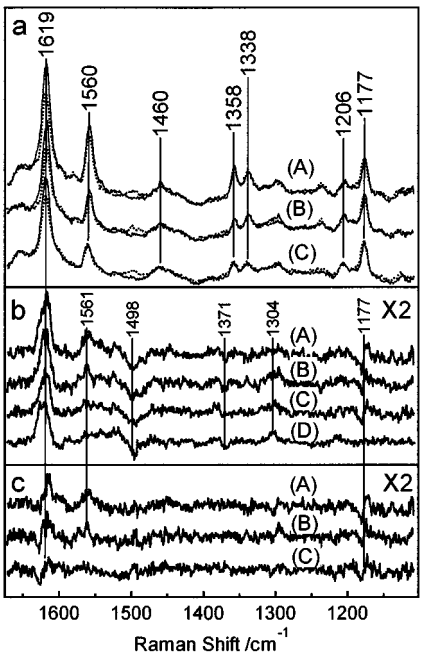

FIGURE 5: Panel a: UVRR spectra of deoxy (solid lines) and CO-bound forms (broken lines) of native swMb (A), the W14F mutant (B), and the W7F mutant (C). Panel b: The deoxy minus CO difference spectra of native swMb (A), W14F (B), W7F (C), and the 2-MeIm adduct of iron porphyrin (D). The ordinate scales are expanded by a factor of 2 compared with those in panel a. Panel c: The double difference spectra, spectra (A−C) minus spectrum (D) of panel b. The ordinate scales are expanded by a factor of 2 compared with those in panel a.

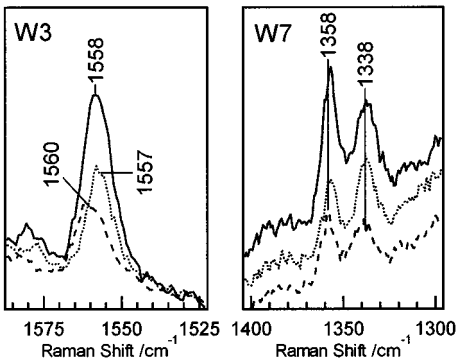

FIGURE 6: Expanded spectra in the W3 and W7 regions of CO-bound native swMb (solid line), the W14F mutant (dotted line), and the W7F mutant (broken line).

spectrum of the heme model compound, and it does not give any difference peak around 1560 cm^{-1}. To demonstrate the protein contribution more clearly, the heme contributions in traces A−C were removed by subtracting trace D from them. The double difference spectra are delineated in Figure 5c. It is evident that the most part of the change of the Trp W3 band of native Mb comes from Trp7. The W3 band of Trp7 (W14F mutant) is slightly shifted to a lower frequency and exhibits intensity reduction upon ligand binding. In addition, the difference peak around 1620 cm^{-1} involves the contribution not only from the vinyl group of the heme but also from Tyr and Trp residues.

More detailed examination of the W3 bands of the W7F and W14F mutants showed an appreciable difference of their peak frequencies. Figure 6 displays the expanded raw spectra of the CO-bound forms of the native (solid line) and W14F (dotted line) and W7F mutants (broken line) in the W3 (left panel) and W7 regions (right panel). The W3 band of Trp7 (W14F mutant) appeared at 1557 cm^{-1} whereas that of Trp14 (W7F mutant) appeared at 1560 cm^{-1}. Since the digital sum of the spectra of Trp7 and Trp14 well reproduced the observed spectrum of native Mb, this difference of frequency is considered to reflect the nature of each Trp residue.

The I_{1358}/I_{1338} intensity ratio of the W7 doublet is known to be sensitive to environments of the indole side chain of the Trp residue, being larger for more hydrophobic environments. This is owed to the fact that the 1358/1338 cm^{-1} doublet arises from Fermi resonance between the N_1C_8 stretching fundamental (W7) and the combination of out-of-plane bending vibrations (*35*). As demonstrated in the right panel of Figure 6, the I_{1358}/I_{1338} ratio of Trp14 is 1.3, which is larger than 1.0 for Trp7, consistent with the fact that Trp14 is buried in a more hydrophobic environment than Trp7. Since the intensity ratio exhibits little change between the deoxy and CO-bound states as shown in Figure 5c, the difference between Trp14 and Trp7 seems to be retained upon ligand binding/dissociation. Because of appreciable contribution from the heme moiety to the difference spectrum in this frequency region, it would be more reliable to use the W3 rather than the W7 band to discuss the environments of Trp residues when a heme is present in the protein.

The pK_a of the distal His of Mb is thought to be 4.4 (*16*). This value is extremely lower than an ordinary value (pK_a = 6.65) (*30*) and might be ascribed to the hydrophobic environments of the heme pocket. On the other hand, the structure of *n*-BuICMb has been solved with X-ray crystallography, reported in the data bank (*36*), which indicated that the distal His is swung up to protein surface. If this position is exposed to solvent, distal His at an appropriate pH might be protonated at the exposed position but not protonated in the heme pocket. Only a protonated histidine is known to yield a UVRR band around 1410 cm^{-1} in D_2O (*29*, *30*). Accordingly, we examined UVRR spectra of COMb and *n*-BuICMb in D_2O between pH 6.4 and pH 4.6, and the results are displayed in Figure 7. Deuterated histidinium in Mb gave a Raman band at 1407 cm^{-1}, and its intensity increased as the pH decreased as shown by spectra A−D in Figure 7. Although the intensity of the 1407 cm^{-1} band of free histidine exhibited no pH dependence below pD 5, that of Mb still increased there due to the presence of His residues with different pK_a values. Nevertheless, the difference spectra between COMb and *n*-BuICMb delineated by traces E and F gave no peak at 1407 cm^{-1} between pD 6.4 and pD 4.6, while differences derived by heme were seen at 1500 and 1370 cm^{-1}.

DISCUSSION

Trp Conformation. In the 244 nm excited UVRR spectra of Mb, some RR bands of heme unexpectedly appeared in addition to RR bands of Tyr and Trp residues. Since they change between the deoxy and ligand-bound states, it is important to get rid of the contribution of the heme from the protein spectra. On the basis of the difference spectra between the deoxy and CO-bound states of the model complex shown in Figure 2, some difference peaks shown in Figure 1 were attributed to the heme moiety; the positive band at 1622 cm^{-1} is assigned to the C═C stretching of vinyl

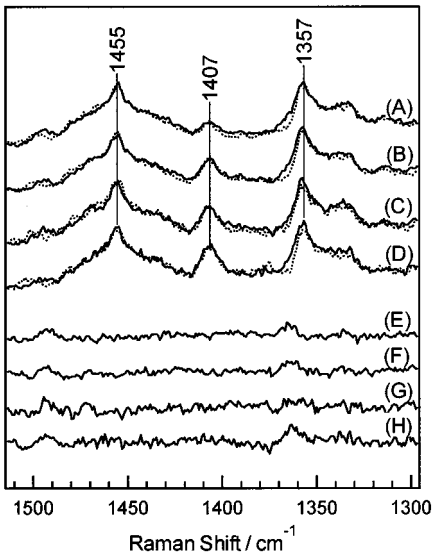

FIGURE 7: UVRR spectra of *n*-BuICMb (solid lines) and COMb (broken lines) at various pD values in D_2O: (A) pD 6.4, (B) pD 5.2, (C) pD 4.9, and (D) pD 4.6. The difference spectra, *n*-BuICMb minus COMb, of spectra A−D are delineated by traces E−H, respectively. The ordinate scales of traces E−H are the same as those of traces A−D. The pD values are regarded as direct reading values on the pH meter.

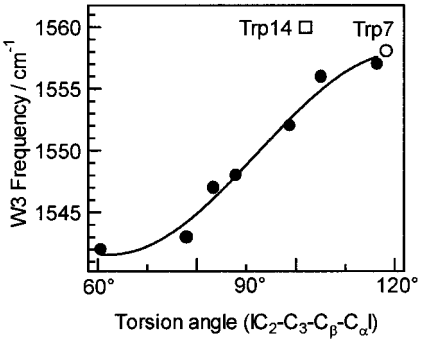

FIGURE 8: Correlation between W3 frequencies and the $C_2-C_3-C_\beta-C_\alpha$ torsional angle (θ) of tryptophan residues found by Miura et al. (*41*). Closed circles denote the original plot (*41*), and the open markers indicate the data obtained in the present study. The solid line shows the curve best fitted in this study using cos(3θ) as a variable.

group of heme side chain (*37*−*40*), and the negative bands at 1495 and 1371 cm^{-1} arise from the ν_3 and ν_4 modes of the porphyrin skeleton, respectively. Although the Trp doublet around 1358/1338 cm^{-1} was overlapped with the heme bands, the W3 band of Trp and the Y9a band of Tyr have no overlapping with heme bands.

It has been pointed out by Miura et al. (*41*) that the W3 frequency of the Trp residue has a good correlation with the torsion angle (θ) of the $C_2-C_3-C_\beta-C_\alpha$ part of indole side chain. The two frequencies thus observed are plotted against the X-ray-determined torsion angles (*6*) and compared with the expected ones in Figure 8, where the solid line denotes the empirical curve newly fitted with cos(3θ) as a variable. While the W3 frequency of Trp7 falls on the empirical curve, the frequency of Trp14 is higher than the expected value. Trp14 is buried in the folded protein, and its environment seems to be more hydrophobic than that of Trp7 as discussed below, but this abnormal frequency and intensity of the W3 band of Trp14 cannot be explained satisfactorily with our current knowledge. One possibility is that a hydrogen bond to the indole nitrogen atom affects this frequency and intensity, and the other is that the torsion angle of $C_3-C_\beta-C_\alpha-N$, which might influence the W3 frequency, is different from those of the Trp model compounds used in the plots (*41*). It is emphasized that the present study provides the first separate detection of individual spectra of Trp7 and Trp14.

Relation with X-ray Results. High-resolution X-ray crystallographic data are available for various states of native and mutant Mbs (*6*, *17*, *42*−*44*). Although the location of Tyr151 is different among several analyses, it can be summarized that Tyr151 has two positions: one is directed toward the F−G loop (inward) and the other is directed toward the F helix (outward). In the recent data with near-atomic resolution, Bartunik and co-workers (*6*) addressed that Tyr151 pointed to the F helix in the CO-bound form but had two directions in the deoxy state, while Phillips and co-workers (*43*) pointed out that Tyr151 had two directions in both states, the occupation density of which was changed in the two states. The common tendency in these two analyses is that Tyr151 is predominantly directed inward in the deoxy state and outward in the CO-bound state. The flexibility and fluctuation of the C-terminus may explain these differences and similarities.

The Y9a band of swMb exhibited the deoxy minus CO difference peak, but that of hMb did not (Figure 3). Therefore, this difference peak is attributed to Tyr151, indicating that Tyr151 of swMb is flexible in the solution and is placed in different environments between the deoxy and CO-bound states. Its frequency is lower and its intensity is higher in the deoxy state than in the CO-bound state. This means that Tyr151 is placed in more hydrophobic environments and works as a hydrogen bond donor in the deoxy state rather than in the CO-bound state on the basis of the results shown in Figure 4. Probably the hydrophobic environments cause a red shift of the electronic La absorption band, approaching the Raman excitation wavelength, and as a result, resonance enhancement of Raman intensity becomes larger upon excitation at 244 nm. Although there was a question whether lattice forces in crystals might prevent the C-terminal flexibility in solution from the tertiary conformational change, the UVRR results for solution are compatible to the X-ray results for crystals, if the inward and outward locations of Tyr151 correspond to the more hydrophobic and hydrophilic environments, respectively, suggesting the absence of large lattice constrain. It is reported that the Y9a frequency depends on the torsion angle of the phenolic C−O−H group of the tyrosine side chain (*45*). Since the distance of Tyr151 directed toward the G−F loop allows to make a hydrogen bond with an oxygen atom of the main chain Lys98, the torsion angle of the hydroxyl group would be changed through the movement of Tyr151.

The importance of the movements of the C-terminal residues has been anticipated from the studies of Hb cooperativity, in which removal of the C-terminal residues such as Arg141α and His146β from HbA raised oxygen affinity and made the oxygen binding equilibrium noncooperative *(46, 47)*. In fact, it was demonstrated by the UVRR study of the Hb quaternary structure (*48*) that the penultimate tyrosines (Tyr140α and Tyr145β) exhibit clear spectral changes upon ligand binding. The present result is consistent

with these features, which seem to be a common basic property of heme proteins.

Open/Close Forms. A pathway of an external ligand from solvent to heme could not be found in the stationary structures of the deoxy and CO-bound forms of Mb. However, X-ray crystallographic studies pointed out that distal His was rotated and swung up toward the protein surface under extreme conditions and that a pathway of a ligand was opened. Such a structure has been found for swMb with bulky ligands such as imidazole (*18*, *49*), phenylhydrazine (*19*), and alkyl isocyanide (*20*) and is regarded as a model of the open form of the pathway. Yang and Phillips, Jr. (*17*), found that a similar open form was produced with COMb at pH 4, owing to the electrostatic interactions between the protonated distal His in the hydrophobic environment of pocket and the bound CO. Due to this structural change, the Fe−CO stretching band of COMb shifts from 507 cm^{-1} at pH 7 to 488 cm^{-1} at pH 4 (*16*). Furthermore, a transient open form was detected in the time-resolved UVRR experiments using CO photolysis of the H64Y mutant (*22*). These studies supported the idea that the movement of the distal His is involved in the open/close changes of a ligand pathway. The UVRR spectrum of the isocyanide adduct of Mb shown in Figure 1C, which is considered to adopt the distal His swung up structure, is unexpectedly very close to that of the CO-bound form (Figure 1B). This means that the movement of His64 is localized around the heme pocket and scarcely affects the overall protein structure.

The N-deuterated imidazolium ring of the histidine residue gave a clear UVRR band at 1407 cm^{-1} for Mb upon excitation at 244 nm. We expected that the open form could be detected if the pK_a of His64 was higher in the open form than in the closed form. The stationary open form is expected to be generated when a large ligand is bound to the heme iron (*18*−*20*, *49*), although it is not expected for COMb above pH 4.4. Accordingly, UVRR spectra of the CO- and *n*-BuIC-bound Mbs were examined at various pD values from 6.4 to 4.6 as shown in Figure 7A−D. Although the intensity of the 1407 cm^{-1} band of deuterated histidyl imidazolium increased at lower pH, no peak was recognized in the difference spectra between the CO- and *n*-BuIC bound forms as depicted by traces E−H in Figure 7. This would mean that the pK_a of His64 within the heme pocket is not so different from that in the position of the open form or alternatively that the S/N ratio in the present experiment was not high enough to extract the contribution of one His residue from the twelve His residues included in swMb.

Conformational Change of Mb upon Ligand Binding. The proximal His is known to play a significant role in the T−R transition of Hb, and much attention has been paid to it (*25*). In contrast, studies on the proximal side of Mb are much less prevalent. Although structural changes of Mb upon ligand binding might be smaller than those of Hb, the present study demonstrated that Trp7 and Tyr151 in the N- and C-terminal regions, respectively, undergo appreciable changes. Mb consists of eight helices, and the heme is embedded between the E and F helices, while Trp7 and Tyr151 are contained in the A and H helices, which are interacting with the E and F helices, respectively. Therefore, some changes in helix−helix interactions must be involved in the ligand biding. Seno and Go (*50*) carried out normal coordinate analysis of deoxyMb and on the basis of 151 modes below 40 cm^{-1} interpreted the atomic displacements of the globin moiety upon ligand binding. The largest displacements were contained in the region from the F helix to the beginning of the G helix, and secondary regions are the A and C helices, the CD corner, the E helix, and the C-terminal side of the H helix. All of the Trp and Tyr residues are contained in the secondary sensitive regions. The appearance of the ligand binding effects only on Trp7 and Tyr151 residues might be partly due to the fact that these side chains are located near the surface of the protein and accordingly are favorable for the detection of slight conformational change and partly due to the fact that the slight structural change of the active site is amplified in proportion to the distance.

Causprove and Dyer (*13*) measured time-resolved FTIR spectra of photolyzed MbCO, pointing out that the change of the amide I band with the time constants of 6−8 ps was mainly due to the proximal side, through the F helix. They deduced that the contribution to the structural change from the distal side was smaller than that from the proximal side. Accordingly, some rearrangements of helix topology caused by movement of the heme iron would be transmitted to Tyr151 in the C-terminus and Trp7 near the N-terminus of the polypeptide chain. This is compatible to the result from the time-resolved fluorescence study, which pointed out appreciable difference in the quenching time of the Trp7 fluorescence between the deoxy and CO forms (*15*).

The present results demonstrate that a structural change of heme upon ligand binding is communicated to the terminal parts of polypeptide chain. While the environmental and structural changes of Trp7 and Tyr151 imply an overall conformational change of the protein, it is difficult to address how this subtle conformational change is connected to the function of Mb. However, it became clear from the present study that a small structural change in the buried portion of a protein causes a rather large conformational change at the surface and can communicate it to an adjacent subunit to regulate its function, such as signal transduction.

REFERENCES

1. Rodgers, K. R. (1999) *Curr. Opin. Chem Biol. 3*, 158−167.
2. He, Y., Gaal, T., Karls, R., Donohue, T. J., Gourse, R. L., and Roberts, G. P. (1999) *J. Biol. Chem. 274*, 10840−10845.
3. Gilles-Gonzalez, M. A., Ditta, G. S., and Helinski, D. R. (1991) *Nature 350*, 170−172.
4. Stone, J. R., and Marletta, M. A. (1996) *Biochemistry 35*, 1093−1099.
5. Delgado-Nixon, V. M., Gonzalez, G., and Gilles-Gonzalez, M. A. (2000) *Biochemistry 39*, 2685−2691.
6. Kachalova, G. S., Popov, A. N., and Bartunik, H. D. (1999) *Science 284*, 473−476.
7. Osapay, K., Theriault, Y., Wright, P. E., and Case, D. A. (1994) *J. Mol. Biol. 244*, 183−197.
8. Causgrove, T. P., and Dyer, R. B. (1993) *Biochemistry 32*, 11985−11991.
9. Sage, J. T., Schomacker, K. T., and Champion, P. M. (1995) *J. Phys. Chem. 99*, 3394−3405.
10. Springer, B. A., Sligar, S. G., Olson, J. S., and Phillips, G. N., Jr. (1994) *Chem. Rev. 94*, 699−714.
11. Olson, J. S., and Phillips, G. N., Jr. (1996) *J. Biol. Chem. 271*, 17593−17596.
12. Olson, J. S., and Phillips, G. N., Jr. (1997) *J. Biol. Inorg. Chem. 2*, 544−552.
13. Causgrove, T. P., and Dyer, R. B. (1996) *J. Phys. Chem. 100*, 3273−3277.

14. Ansari, A., Jones, C. M., Henry, E. R., Hofrichter, J., and Eaton, W. A. (1994) *Biochemistry 33*, 5128−5145.
15. Gryczynski, Z., and Bucci, E. (1998) *Biophys. Chem. 74*, 187−196.
16. Ramsden, J., and Spiro, T. G. (1989) *Biochemistry 28*, 3125−3128.
17. Yang, F., and Phillips, G. N., Jr. (1996) *J. Mol. Biol. 256*, 762−774.
18. Bolognesi, M., Cannillo, E., Ascenzi, P., Giacometti, G. M., Merli, A., and Brunori, M. (1982) *J. Mol. Biol. 158*, 305−315.
19. Ringe, D., Petsko, G. A., Kerr, D. E., and Ortiz de Montellano, P. R. (1984) *Biochemistry 23*, 2−4.
20. Johnson, K. A., Olson, J. S., and Phillips, G. N., Jr. (1989) *J. Mol. Biol. 207*, 459−463.
21. Lai, H. H., Li, T., Lyons, D. S., Phillips, G. N., Jr., Olson, J. S., and Gibson, Q. H. (1995) *Proteins 22*, 322−339.
22. Mukai, M., Nakashima, S., Olson, J. S., and Kitagawa, T. (1998) *J. Phys. Chem. 102*, 3624−3630.
23. Hu, X., Rodgers, K. R., Mukerji, I., and Spiro, T. G. (1999) *Biochemistry 38*, 3462−3467.
24. Matsukawa, S., Mawatari, K., Yoneyama, Y., and Kitagawa, T. (1985) *J. Am. Chem. Soc. 107*, 1108−1113.
25. Kitagawa, T. (1988) in *Biological Applications of Raman Spectroscopy* (Spiro, T. G., Ed.) pp 97−131, Wiley, New York.
26. Austin, J. C., Rodgers, K. R., and Spiro, T. G. (1993) in *Method in Enzymology* (Riordan, J. F., and Vallee, B. L., Eds.) pp 374−396, Academic Press, San Diego, CA.
27. Kitagawa, T. (1992) *Prog. Biophys. Mol. Biol. 58*, 1−18.
28. Harada, I., and Takeuchi, H. (1986) *Adv. Spectrosc.: Spectrosc. Biol. Syst.*, 113−175.
29. Lord, R. C., and Yu, N. T. (1970) *J. Mol. Biol. 51*, 203−213.
30. Tasumi, M., Harada, I., and Takamatsu, T. (1982) *J. Raman Spectrosc. 12*, 149−151.
31. Springer, B. A., Egeberg, K. D., Sligar, S. G., Rohlfs, R. J., Mathews, A. J., and Olson, J. S. (1989) *J. Biol. Chem. 264*, 3057−3060.
32. Aki, M., Ogura, T., Shinzawa-Itoh, K., Yoshikawa, S., and Kitagawa, T. (2000) *J. Phys. Chem. 104*, 10765−10774.
33. Evans, S. V., and Brayer, G. D. (1988) *J. Biol. Chem. 263*, 4263−4268.
34. Uyeda, M., and Peisach, J. (1981) *Biochemistry 20*, 2028−2035.
35. Harada, I., Miura, T., and Takeuchi, H. (1986) *Spectrochim. Acta 42A*, 307−312.
36. Smith, R. D., Olson, J. S., and Phillips, G. N., Jr. (1997) X-ray structure of *n*-BuICMb was referred from Protein Data Bank, PDB code 104M.
37. Choi, S., Spiro, T. G., Langry, K. C., Smith, K. M., Budd, D. L., and La Mar, G. N. (1982) *J. Am. Chem. Soc. 104*, 4345−4351.
38. Choi, S., Spiro, T. G., Langry, K. C., and Smith, K. M. (1982) *J. Am. Chem. Soc. 104*, 4337−4344.
39. Devito, V. L., and Asher, S. A. (1989) *J. Am. Chem. Soc. 111*, 9143−9152.
40. Devito, V. L., Cai, M., Asher, S. A., Kehres, L. A., and Smith, K. M. (1992) *J. Phys. Chem. 96*, 6917−6922.
41. Miura, T., Takeuchi, H., and Harada, I. (1989) *J. Raman Spectrosc. 20*, 667−671.
42. Vitkup, D., Petsko, G. A., and Karplus, M. (1997) *Nat. Struct. Biol. 4*, 202−208.
43. Quillin, M. L., Arduini, R. M., Olson, J. S., and Phillips, G. N., Jr. (1993) *J. Mol. Biol. 234*, 140−155.
44. Vojtechovsky, J., Chu, K., Berendzen, J., Sweet, R. M., and Schlichting, I. (1999) *Biophys. J. 77*, 2153−2174.
45. Takeuchi, H., Watanabe, N., Satoh, Y., and Harada, I. (1989) *J. Raman Spectrosc. 20*, 233−237.
46. Kilmartin, J. V., Hewitt, J. A., and Wooton, J. F. (1975) *J. Mol. Biol. 93*, 203−218.
47. Fung, L. W.-M., and Ho, C. (1975) *Biochemistry 14*, 2526−2535.
48. Nagai, M., Wajcman, H., Lahary, A., Nakatsukasa, T., Nagatomo, S., and Kitagawa, T. (1999) *Biochemistry 38*, 1243−1251.
49. Lionetti, C., Guanziroli, M. G., Frigerio, F., Ascenzi, P., and Bolognesi, M. (1991) *J. Mol. Biol. 217*, 409−412.
50. Seno, Y., and Go, N. (1990) *J. Mol. Biol. 216*, 111−126.

BI002640K